IEEE International Conference on Robotics and Automation (ICRA), 2011

Granular lift forces predict vertical motion of a sand-swimming robot

Ryan D. Maladen, Paul B. Umbanhowar, Yang Ding, Andrew Masse, and Daniel I. Goldman

***Abstract*— Previously we modeled the undulatory subsurface locomotion of the sandfish lizard with a sand-swimming robot which displayed performance comparable to the organism. In this work we control the lift forces on the robot by varying its head shape and demonstrate that these granular forces predict the vertical motion of the robot. Inspired by the tapered head of the sandfish lizard, we drag a wedge shaped object horizontally and parallel to its lower face through a granular medium and show that by varying the angle of the upper leading surface of the wedge, α, the lift force can be varied from positive to negative. Testing the robot with these wedges as heads results in vertical motion in the same direction as the lift force in the drag experiments. As the robot moves forward, the force on its head normal to the body plane results in a net torque imbalance which pitches the robot causing it to rise or sink within the medium. Since repeatedly varying α for a wedge head to achieve a desired lift is impractical, we test robot heads that approximate a wedge head inclined at varying angles by changing the angle of the bottom and top surfaces of the wedge, and show that similar lift control is achieved. Our results provide principles for the construction of robots that will be able to follow arbitrary trajectories within complex substrates like sand, and also lend support to hypotheses that morphological adaptations of desert-dwelling organisms aid in their subsurface locomotion.**

I. Introduction

Major advances in creating high performance flying and swimming devices have been made by studying the interaction between airfoils like wings, blade, sails, and keels, and the surrounding fluid (air or water) [1], [2]. Specifically, an understanding of the effects of shape and attack angle on lift have helped design devices that can move vertically in water and air, while minimizing drag forces.

In the biological world swimming and flying organisms enhance performance (e.g. speed and stability) by controlling flow to manipulate lift and drag [3], [4]. Control can be realized passively through the anatomy of the animal (morphological and structural features that dictate flow); examples include protuberances on whale flippers and riblets on shark skin. Control can also be active; fish alter tail camber, area, and angle of attack during tail beat to vary performance [3], [5], while flying insects and birds steer and maneuver largely by varying stroke kinematics (like wing stroke amplitude, attack angle, and timing and duration of wing rotation) to alter the forces and moments generated during forward flight and hovering [6], [7], [8]. Developing a robot that can move within complex flowing environments (e.g. sand, soil, and leaf-litter) is challenging as these types of substrates can display both solid and fluid-like behavior in response to stress. Robots able to navigate such environments could find application as search and rescue devices within rubble following earthquakes or mine collapses [9], [10], [11], or within desert sand to identify land mines. Presently, design of such devices is challenging since a validated theoretical framework comparable to continuum theories at the level of the Navier-Stokes equations for fluids [12] does not exist.

Experiments on slow horizontal and vertical drag [13], [14] of objects within granular media have provided some understanding of the observed drag forces, but few have investigated the associated lift forces. Studies have examined the scaling of the lift force with intruder depth and width for a partially submerged vertical rod moving horizontally [15] and a rotating plate [16], the drag force on submerged objects with curved surfaces [13], and, recently, the lift forces acting on horizontally translated submerged objects [17].

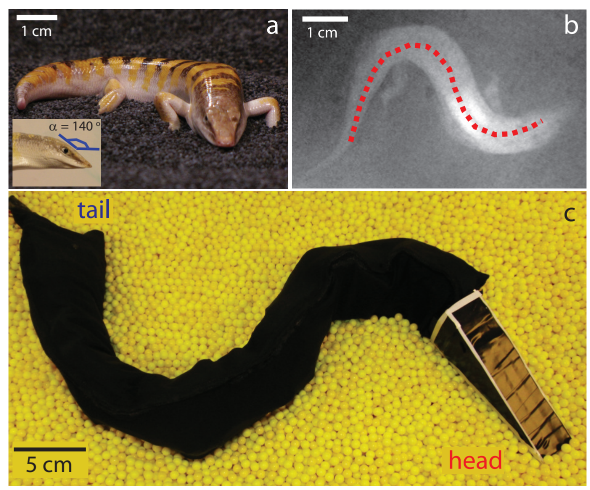

Fig. 1. (a) The sandfish *Scincus scincus*, a sand-swimming lizard that inhabits the Saharan desert. Inset shows a side view of the wedge-like sandfish head. (b) X-ray image of sandfish swimming subsurface in 0.3 mm spherical glass particles. Red dashed curve marks tracked mid-line. See [18] for details on sandfish kinematics. (c) The six motor, seven segment robot with a wedge shaped head ($\alpha = 155°$) studied here.

Intuition for factors affecting navigation of challenging environments may be obtained by studying desert organisms like scorpions, snakes, and lizards that burrow and swim effectively in sand [19], [20], [21], [22] to escape heat and predators, and hunt for prey [23], [24]. Certain morphological adaptations of these organism, e.g. a shovel

R. D. Maladen is with the Bioengineering Program, and Y. Ding, A. Masse, and D. I. Goldman are with the School of Physics at the Georgia Institute of Technology, Atlanta, GA 30332, USA. {rmaladen,dingyang,amasse}@gatech.edu, daniel.goldman@physics.gatech.edu.

P. B. Umbanhowar is with the Department of Mechanical Engineering, Northwestern University, Evanston, IL 60208, USA. umbanhowar@northwestern.edu.

shaped snout [25], [23], have been hypothesized to reduce drag during sand-swimming.

Motivated by high speed x-ray imaging studies [18] and models [26] elucidating the mechanics of rapid subsurface locomotion of a sand-swimming lizard, and challenged by the absence of robotic devices with subterranean locomotor abilities comparable to desert adapted organisms, we previously developed a biophysically inspired sand-swimming device [27], [28]. Here, inspired by the morphology of the sandfish lizard (Fig. 1 a), and guided by object drag experiments in granular media [17], we demonstrate that lift forces depend on intruder shape and study the effect these shapes have on the trajectory of the robot. To avoid the inconvenience of varying head shape to vary lift and to keep the experiments relevant to the biological organism, we also test robot head shapes that approximate a fixed head shape tilted at various angles to modulate lift.

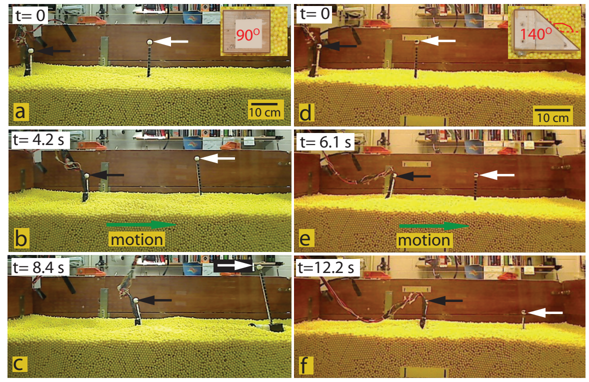

Fig. 2. (a-c) Square head robot [27], [28] and (d-f) robot with a wedge shaped head ($\alpha = 140°$) swimming subsurface in 6 mm plastic particles. Insets in (a) and (d) show the robot head. Black and white arrows mark the mast mounted spheres at the robot's tail and head used to track the robot's position and orientation.

II. Sand-swimming robot

A. *Design overview and methods*

The body of the sand-swimming robot (adapted from previously developed snake robots [29]) consists of single axis motors oriented to allow angular excursions in the body plane and connected via identical links. Our design employs six standard size ($4 \times 3 \times 3.7$ cm^3) servomotors (Hitec, HSR 5980SG) and a passive segment (the head) with the weight, width, and height of a motor for a total of seven segments (Fig. 1 c). To reduce motor torque requirements, we use low friction 6 mm plastic particles (density= 1.03 g/cm^3) as our granular medium. The granular bed is $110 \times 40 \times 30$ cm^3 in extent. Details of the experimental setup are in [27], [28]. Simultaneous top and side view videos (30 fps) are collected for each condition tested. To track the robot position subsurface, a mast with a spherical marker is attached to the first and last segments and oriented normal to the body plane. Before each run the top of the robot is submerged 4 cm into the medium and the surface leveled. The robot position is tracked until either the robot reaches the end of the container or any part of the robot other than the mast reaches the surface.

B. *Robot kinematic control: traveling vs. standing waves*

The robot kinematics, inspired by the undulatory kinematics of the sandfish lizard [18], are prescribed by a feed-forward controller that modulates the angle between adjacent segments as

$$\beta(i,t) = \beta_0 \xi \sin(2\pi\xi i/N - 2\pi f t), \qquad (1)$$

where $\beta(i,t)$ is the motor angle of the i^{th} motor at time t, β_0 is the angular amplitude, f the oscillation frequency, ξ the number of wavelengths along the body (period), and N the number of motors. The robot is tested for fixed kinematic parameters of $f = 0.25$ Hz, amplitude/wavelength$= 0.2$, and $\xi = 1$.

Our previous studies [27], [28] found that the square head robot rose to the surface of the media within $2-3$ cycles (see Fig. 2 a-c). To ensure that this phenomenon was not an artifact of a torque imbalance resulting from the wires tethered to the robot tail mast, we reversed the direction of the traveling wave along the robot such that the tail became the head and found that again the leading segment rose. Hydrostatic buoyancy was also discarded as an explanation as the robot experienced no lift unless it moved through the medium, and the ratio of the density of the robot to the plastic particles, 1.16 was greater than one. Also, the observed surfacing behavior is different from the Brazil nut effect [30] in which lift results from agitation of the medium by the container.

To determine whether lateral or forward motion of the robot produces the observed lift, we tested the robot with standing wave kinematics given as

$$\beta(i,t) = \beta_0 \xi \sin(2\pi f t) \sin(2\pi\xi i/N). \qquad (2)$$

As expected, the robot did not progress forward due to the symmetry of this undulatory motion. More interestingly, and contrary to the observations for the traveling wave kinematics, the robot did not rise (Fig. 3 a). This indicated that forward motion is necessary for the robot to rise and motivated our investigation on the effect of head shape on the vertical motion of the robot.

III. Drag induced lift in granular media

We first test the effect of wedge shapes on the lift forces induced as they are dragged through granular media. Inspired by the head shape of the sandfish lizard (Fig. 1 a inset), we confine our drag testing to objects (Group I, see Fig. 4 a) for which the angle of the upper leading surface (α) is varied while the height and projected front and lateral areas remain fixed. Extremes of α were limited to the largest head length that would not interfere with the sides of the container during undulatory motion (see Section IV). The weight of each wooden wedge was controlled to match the square head (110 g) by adding lead to the hollowed out heads.

Each wedge was dragged horizontally with its bottom face horizontal through a container ($40 \times 30 \times 24$ cm^3) filled with

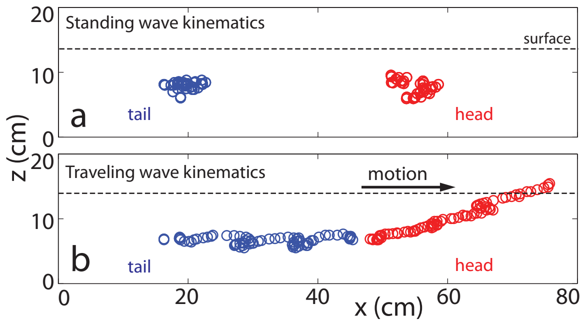

Fig. 3. The square head robot [27], [28] (a) does not rise or advance with standing wave kinematics but (b) does rise and advance with traveling wave kinematics. The red and blue symbols correspond to the tracked position of the head and tail respectively as the robot swims subsurface for ≈ 3 cycles of motion. Dashed line indicates the top surface of the container.

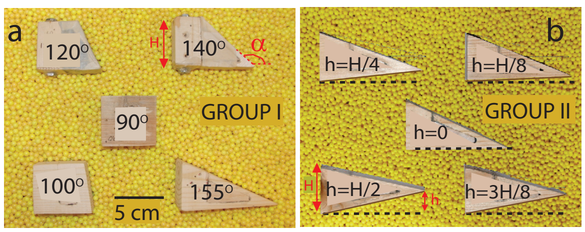

Fig. 4. Top view of head shapes tested in physics drag and robot experiments resting on 6 mm plastic particles. All objects have fixed height ($H = 5$ cm) and transverse projected area = 27.5 cm^2. (a) Group I: objects with fixed lateral projected area for various wedge angles α. Each object reflected horizontally corresponds to objects with $\alpha = 180°$ minus the labeled α. (b) Group II: objects with fixed length (11 cm) with vertical position of the leading edge (h) varying as a fraction of $H = 5$ cm. See text (Section III) for detailed description of objects.

the same 6 mm plastic particles used in the robot experiment (Fig. 5 inset). Since forces in granular media are independent of speed in the range of interest (force changes by less than 10% for speeds < 40 cm/s in 0.3 mm glass particles [18]) drag tests in experiment were performed at a constant speed of 5 cm/s with the wedge's vertical mid-point at depth $d =$ 6.5 cm and its long axis parallel to the motion direction. Each wedge was attached to a robotic arm (CRS Robotics) via a thin but stiff supporting rod and moved by the arm at a constant depth and velocity while a 6 d.o.f. force sensor (ATI industrial) mounted between the robotic arm and the supporting rod measured the drag and lift force. Force on the supporting rod was measured separately and subtracted to obtain the force on the object alone. Tests were repeated three times for each object.

We found that as hypothesized in the biological literature a streamlined head shape reduced the drag force [25], [23]. The reduction in drag between a square head, $\alpha = 90°$, and a head shape with $\alpha = 140°$ (similar to the animal) was nearly 20%. Remarkably, drag reduction was not the dominant effect of 'stream-lining' the head shape; lift forces increased by nearly an order of magnitude, and even changed direction. Specifically, we found that the lift force of the square head ($\alpha = 90°$) is positive, indicating that if vertically

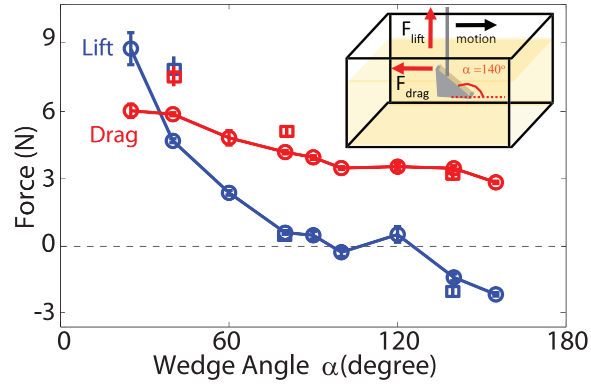

Fig. 5. Measured lift (blue) and drag (red) force on wedge shaped objects (Group I) ($25° < \alpha < 155°$) translated at a depth (top of object to surface) of 4 cm through 6 mm plastic particles. Circle and square symbols correspond to experimental and DEM simulated forces, respectively. Inset: schematic of the experiment.

unconstrained the object would rise to the surface when moved forward. This agrees with our observations for the robot (Fig. 3 b). The vertical force on the object is positive for $\alpha < 80°$, negative for $\alpha > 120°$, and nearly zero for intermediate α ($80° < \alpha < 120°$) (Fig. 5).

To gain an understanding of the measured granular lift forces, we drag three representative shapes through a multi-particle Discrete Element Method (DEM) simulation of the same granular medium used in the drag experiments (6 mm plastic particles). The simulation predicts average drag and lift forces to within 10% over the range of wedge angles studied. As in [17], we found the drag and lift on these intruders results mainly from the force on the leading surface of the object, as forces on surfaces parallel to the direction of motion are small (Fig. 6). On the leading surface, the normal force is larger than the tangential force (the friction force). Positive lift corresponds to $\alpha < 90°$ and negative lift corresponds to $\alpha > 90°$. The magnitudes of the drag and lift forces are larger for $\alpha < 90°$ because the inclined surface pushes the media downward where the yield stress is larger. The increases of yield stress in granular media also makes the flow asymmetric such that for all shapes most particles in front of the intruder rise. For the square shape this upward flow generates a small lift via the friction force on the leading surface. For further details on the physics of granular drag, see [17].

IV. Robot head shape variation

Motivated by our observations of how lift force varies with the shape of the dragged object, we use the objects in Group I (Fig. 4 a) as robot heads and test how their shape affects the trajectory of the robot in the vertical plane (Fig. 7). For each test, we measure the rate of vertical displacement of the center of mass of the robot (cm/cycle).

We found that similar to the results in Section III, the robot moves upward or downward depending on the head shape; the direction is in agreement with the force measurements on the individual isolated heads. We hypothesize that the robot

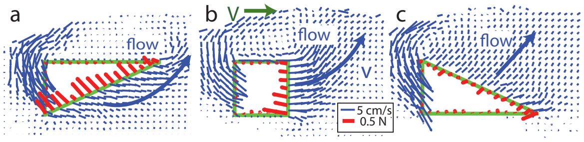

Fig. 6. Numerical simulation of objects dragged through experimentally validated 6 mm plastic particles. (a), (b), and (c) correspond to $\alpha = 40°$, $90°$, and $140°$ respectively. Red and blue lines denote the magnitude and direction of force on the surface of the objects and the velocity of the particles respectively. Thick blue arrows indicate the average direction of flow where velocity is averaged over 0.8 cm×0.8 cm cells along the thickness of the plate (into the page) and two time instants separated by a horizontal displacement of 0.05 cm. The force is similarly averaged except the volume is replaced by an area on the surface of the intruder.

head experiences a lift force which results in a torque imbalance which causes the robot to pitch and rise to the surface for head shapes with $\alpha < 90°$, but descend into the medium for $\alpha > 120°$ (see Fig. 2 d-f). For $100° < \alpha < 120°$, the robot does not move vertically until it encounters the end of the container. The forward speed for head shapes for which the robot did not rise was 0.28 ± 0.02 body-length/cycle independent of oscillation frequency, approximately the same as measured in [27], [28]. We also found for a given head shape the rate of rise of the robot was independent of frequency (and thus also velocity); we therefore limited our testing to $f = 0.25$ Hz. Testing the robot's ability to dive deeper than ≈ 15 cm from the surface was not possible for our initial conditions due to motor torque limitations.

Increasing the length of the longest dimension of the robot head to modulate α is not a practical method to actively control force. A more practical mechanism of trajectory control is to vary the inclination of the robot's head relative to the body plane which is equivalent to varying α.

We test this mechanism with a second set of head shapes (Fig. 4 b, Group II), for which angle of both the upper and lower face of the wedge are varied, while keeping the height, length, and projected front and lateral areas fixed. These head shapes, by varying h between zero and half the height of the wedge ($H/2$), approximate the variations in α caused by an inclined head (Fig. 8 inset). For these head shapes, the height, and projected front and lateral area are the same as the Group I shapes, and the length of the head is the same as the Group I wedge with $\alpha = 155°$.

For Group II head shapes with $h = 0$, the robot progresses downward into the media. For $h = H/4$, although the robot moves forward there is no motion in the vertical plane. Contrary to a symmetric object moving in a fluid which experiences no lift, the symmetric head shape in granular media ($h = H/2$) causes the robot to pitch upward.

We find that the forces on the Group II shapes can be understood as sums of forces on the Group I shapes, similar to the method used in [18] to calculate net drag and thrust on an undulatory sand-swimmer in the horizontal plane. The Group II head shapes may be decomposed into two Group I shapes joined at their bases: the net drag and lift is then a sum of the forces on each face. For the symmetric wedge, α for the top and bottom wedges are $170°$ and $10°$ which

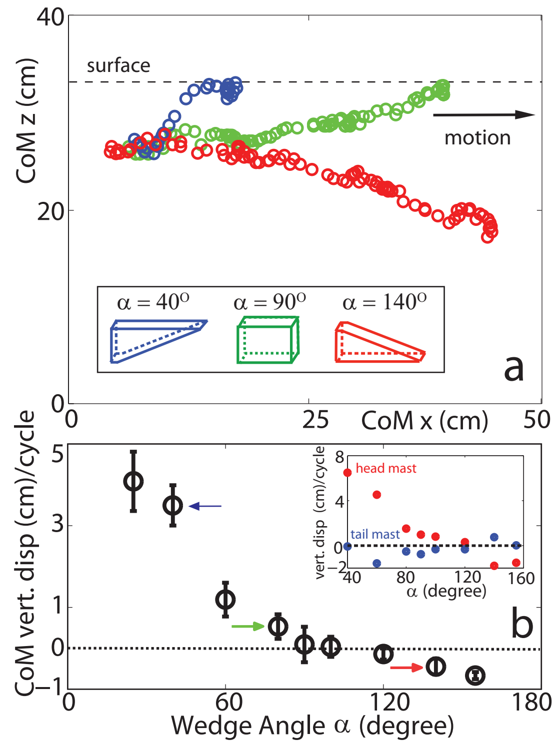

Fig. 7. Robot with Group I head shapes. (a) X-Z trajectories of center of mass (CoM) for α equal $40°$ (blue), $90°$ (green), and $140°$ (red). The CoM was estimated from the average positions of the head and tail segments. The angle of the masts relative to the vertical were considered when calculating the positions of the head and tail segments at each time instant. Inset: head shapes. (b) Average vertical displacement of CoM per cycle ($N = 3$ runs) vs. wedge angle α.

produces a net positive lift force and explains the robot's upward motion.

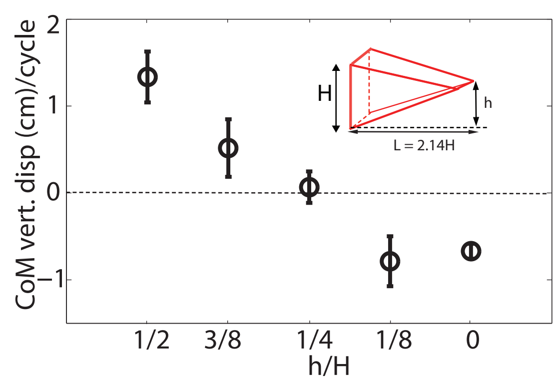

Fig. 8. Robot with Group II head shapes. Lift per cycle for robot with heads in Fig. 4 b. Inset shows head dimensions. Height H and length L of the wedge were fixed at 5 cm and 11 cm, respectively and correspond to the Group I wedge with $\alpha = 155°$ tested in Section IV a.

Having identified robot head shapes that produce either positive, negative or zero displacement of the center of mass as it progresses forward, we now describe further details of the robot kinematics (see Fig. 9). The sign of the vertical displacement per cycle for a given head shape is predicted by the sign of the lift force on the isolated head. This force presumably results in a torque imbalance which causes the robot to change its pitch (at angle γ) about the tail segment which raises or lowers the center of mass. The lift force generated at the head varies with head shape while the lift force at the tail remains constant and effectively zero (Fig. 7 inset). For head shapes with positive lift, the robot's head always exited the material first, and the tail only rose after the head reached the surface.

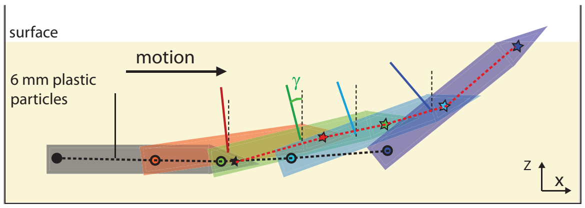

Fig. 9. Schematic of robot ($h > H/4$) swimming within granular media. Different colors indicate the position of the robot as it advances in time. Dashed red and black lines connecting circles and stars correspond to the position of the head and tail segments of the robot, respectively. Lines perpendicular to the robot body indicate the pitch (γ).

Tracking the pitching of the robot tested with Group I head shapes reveals that γ increases as the robot progresses forward for all head shapes tested (Fig. 10 a).

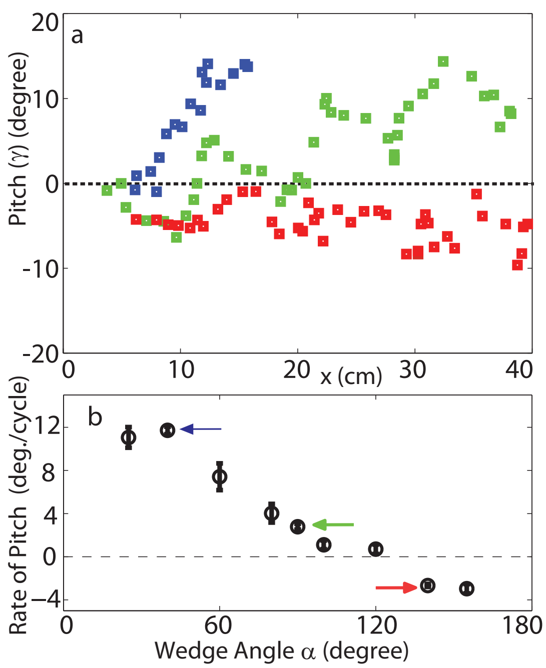

Fig. 10. Pitch of robot vs. forward displacement. (a) Blue, green, and red squares correspond to the robot with α equal to 40°, 90°, and 140°. (b) Change in pitch per cycle measured for Group I heads tested in Section IV a.

V. Discussion

Motivated by research on the interaction between locomotors (animals and robots) and fluids, the present work is the first to explore the analogous effects of lift and drag forces on a robot swimming within a granular medium. Low Reynolds (Re) number fluids are similar to granular media in that drag and lift in both are dominated by non-inertial forces. However, the interaction between object and environment (relevant to lift force production) is quite different in each regime. First, unlike low Re fluids where forces depend on velocity (Stoke's law [12]), in granular media forces are independent of velocity. Second, as an object moves within a granular medium the particles mainly flow upward and the material's yield stress (which determines the magnitude of the lift force) increases with depth. In fluids however, no yield stress exists, and the fluid-object interactions are independent of depth. So, contrary to a symmetric object moving in a fluid which experiences no lift, the symmetric head shape in granular media generates positive lift.

The ability to control the vertical position of a robot by choosing an appropriate head shape and modulating its inclination opens up avenues for further research into maneuvering in sand. Side view x-ray images of the sandfish lizard, which has a wedge shaped head with $\alpha \approx 140°$, reveal that it swims into 0.3 mm glass particles at nearly constant angle of descent $\approx 20°$ (Fig. 11). Our present study shows that an object with the animal's head shape moves downward as it progresses forward. We intend to test the hypothesis that the animal must vary its head angle and effectively α to realize a straight trajectory.

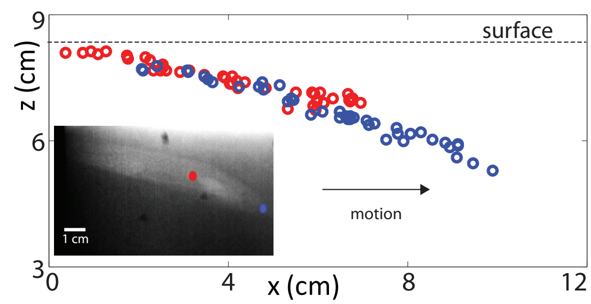

Fig. 11. Kinematics of a sandfish lizard obtained from side-view x-ray imaging. Blue and red circles correspond to the positions of the animal's snout and $\approx 40\%$ of its body-length measured from its snout, respectively. The animal maintains a straight trajectory without pitching as it dives into the granular medium. Inset: side view x-ray image of the sandfish within 0.3 mm glass particles.

We observed that when a robot with a head that experiences no lift (when oriented in the horizontal plane) is placed out of plane it rises or sinks based on the orientation of its head with respect to gravity. Of immediate interest is a systematic study of this effect combined with a study of the physics of lift when wedges are dragged along non-horizontal trajectories into medium.

VI. Conclusions

We have identified head shapes that control the vertical motion of a sand-swimming robot as it swims forward within a granular medium. The direction of vertical motion of the undulatory swimming for a given head shape is well-predicted by measurements of drag force on uniformly translating isolated head shapes. For wedge shapes with $\alpha < 100°$ the robot rises to the surface while for $\alpha > 120°$ the robot moves deeper into the media. We also showed that lift can be controlled by varying the inclination of the robot head with respect to its body plane. These results will aid the construction of robots that can maneuver effectively within complex environments. Biologically our results will improve understanding of how the shapes of burrowing and swimming organisms allow them to take advantage of the solid and fluid-like properties of granular media to move effectively within these substrates.

VII. Acknowledgments

The authors acknowledge funding from The Burroughs Wellcome Fund Career Award at the Scientific Interface, NSF Physics of Living Systems grant PHY-0749991, and the Army Research Laboratory (ARL) Micro Autonomous Systems and Technology (MAST) Collaborative Technology Alliance (CTA) under cooperative agreement number W911NF-08-2-0004.

References

[1] H. Kim, D. Shim, and S. Sastry, “Flying robots: modeling, control and decision making,” in *IEEE International Conference on Robotics and Automation, 2002. Proceedings. ICRA'02*, vol. 1, 2002.

[2] M. H. Dickinson, C. T. Farley, R. J. Full, M. A. R. Koehl, R. Kram, and S. Lehman, “How animals move: An integrative view,” *Science*, vol. 288, p. 100, 2000.

[3] F. Fish and G. Lauder, “Passive and active flow control by swimming fishes and mammals,” *Annual Review of Fluid Mechanics*, p. 38, 2006.

[4] F. Fish, “Wing design and scaling of flying fish with regard to flight performance,” *Journal of Zoology*, vol. 221, no. 3, pp. 391–403, 1990.

[5] G. Lauder and P. Madden, “Learning from fish: kinematics and experimental hydrodynamics for roboticists,” *International Journal of Automation and Computing*, vol. 3, no. 4, pp. 325–335, 2006.

[6] S. Sane and M. Dickinson, “The control of flight force by a flapping wing: lift and drag production,” *Journal of Experimental Biology*, vol. 204, no. 15, p. 2607, 2001.

[7] M. Wortmann and W. Zarnack, “Wing movements and lift regulation in the flight of desert locusts,” *Journal of Experimental Biology*, vol. 182, pp. 57–69, 1993.

[8] B. Tobalske, “Biomechanics of bird flight,” *Journal of Experimental Biology*, vol. 210, no. 18, p. 3135, 2007.

[9] G. Metternicht, L. Hurni, and R. Gogu, “Remote sensing of landslides: An analysis of the potential contribution to geo-spatial systems for hazard assessment in mountainous environments,” *Remote sensing of Environment*, vol. 98, no. 2-3, pp. 284–303, 2005.

[10] A. Ashcheulov, I. Gutsul, and V. Maevski, “Device for monitoring the radiation temperature in coal mines,” *Journal of Optical Technology*, vol. 67, no. 3, p. 281, 2000.

[11] H. Choset, J. Luntz, E. Shammas, T. Rached, D. Hull, and C. Dent, “Design and motion planning for serpentine robots,” in *Proceedings of SPIE*, vol. 3990, 2000, p. 148.

[12] D. Tritton, *Physical Fluid Dynamics*. Oxford University Press, 1989.

[13] R. Albert, M. A. Pfeifer, A. L. Barabasi, and P. Schiffer, “Slow drag in a granular medium,” *Physical Review Letters*, vol. 82, no. 1, pp. 205–208, 1999.

[14] D. Goldman and P. Umbanhowar, “Scaling and dynamics of sphere and disk impact into granular media,” *Physical Review E*, vol. 77, no. 2, p. 21308, 2008.

[15] K. Wieghardt, “Experiments in granular flow,” *Annual Review of Fluid Mechanics*, vol. 7, pp. 89–114, 1975.

[16] R. Soller and S. Koehler, “Drag and lift on rotating vanes in granular beds,” *Physical Review E*, vol. 74, no. 2, p. 21305, 2006.

[17] Y. Ding, N. Gravish, and D. I. Goldman, “Drag induced lift in granular media,” *Phys. Rev. Lett.*, vol. 106, no. 2, p. 028001, Jan 2011.

[18] R. Maladen, Y. Ding, C. Li, and D. Goldman, “Undulatory Swimming in Sand: Subsurface Locomotion of the Sandfish Lizard,” *Science*, vol. 325, no. 5938, p. 314, 2009.

[19] F. Meysman, J. Middelburg, and C. Heip, “Bioturbation: a fresh look at Darwin's last idea,” *Trends in Ecology & Evolution*, vol. 21, no. 12, pp. 688–695, 2006.

[20] R. Seymour, P. Withers, and W. Weathers, “Energetics of burrowing, running, and free-living in the Namib Desert golden mole (Eremitalpa namibensis),” *Journal of Zoology*, vol. 244, no. 01, pp. 107–117, 2001.

[21] L. Fielden, “Home range and movement of the Namib Desert golden mole, Eremitalpa granti namibensis(Chrysochloridae).” *Journal of Zoology*, vol. 223, no. 4, pp. 675–686, 1991.

[22] B. Jayne and M. Daggy, “The effects of temperature on the burial performance and axial motor pattern of the sand-swimming of the Mojave fringe-toed lizard Uma scoparia,” *Journal of Experimental Biology*, vol. 203, no. 7, p. 1241, 2000.

[23] E. Arnold, “Identifying the effects of history on adaptation: origins of different sand-diving techniques in lizards,” *J. Zool., Lond*, vol. 235, pp. 351–388, 1995.

[24] C. White, “The influence of foraging mode and arid adaptation on the basal metabolic rates of burrowing mammals,” *Physiological and Biochemical Zoology*, vol. 76, no. 1, pp. 122–134, 2003.

[25] W. Mosauer, “Adaptive convergence in the sand reptiles of the Sahara and of California: a study in structure and behavior,” *Copeia*, pp. 72–78, 1932.

[26] R. Maladen, Y. Ding, A. Kamor, P. Umbanhowar, and D. Goldman, “Mechanical models of sandish locomotion reveal principles of high performance subsurface sand-swimming,” *Journal of The Royal Society Interface, In press*, 2011.

[27] R. Maladen, Y. Ding, P. Umbanhowar, A. Kamor, and D. Goldman, “Biophysically inspired development of a sand-swimming robot,” in *Proceedings of Robotics: Science and Systems*, Zaragoza, Spain, June 2010.

[28] R. Maladen, Y. Ding, P. Umbanhowar, and D. Goldman, “Undulatory swimming in sand: experimental and simulation studies of a robotic sandfish.” *International Journal of Robotics Research, in press*, 2011.

[29] K. Dowling, “Limbless locomotion: learning to crawl,” in *1999 IEEE International Conference on Robotics and Automation, 1999. Proceedings*, vol. 4, 1999.

[30] A. Rosato, K. Strandburg, F. Prinz, and R. Swendsen, “Why the Brazil nuts are on top: Size segregation of particulate matter by shaking,” *Physical Review Letters*, vol. 58, no. 10, pp. 1038–1040, 1987.